THE JOURNAL OF PHYSICAL CHEMISTRY C

Article

pubs.acs.org/JPCC

First Principles Tafel Kinetics for Resolving Key Parameters in Optimizing Oxygen Electrocatalytic Reduction Catalyst

Guang-Feng Wei, Ya-Hui Fang, and Zhi-Pan Liu*

Shanghai Key Laboratory of Molecular Catalysis and Innovative Materials, Department of Chemistry, Key Laboratory of Computational Physical Science (Ministry of Education), Fudan University, Shanghai 200433, China

Supporting Information

ABSTRACT: Oxygen reduction is a critical reaction in the global energy cycle and a vital catalytic process in fuel cells. To date, the atomic level picture on how oxygen is electrocatalytically reduced on the traditional Pt catalyst is not established yet and the design of both active and economic catalysts remains a great challenge. Here first principles based theoretical methods can for the first time resolve the Tafel behavior and the polarization kinetics for oxygen reduction reaction (ORR) on Pt in aqueous soundings and reveal the origin of some key problems, mainly associated with the low intrinsic activity and the rapid poisoning of the electrocatalyst. The atomic level mechanism of ORR on Pt at the concerned potentials (~0.8 V) is established, in which the critical surface coverage to achieve the reaction equilibrium is identified to be 0.25 ML O coverage. From the computed Tafel curve, the proton-coupled O−O bond breaking, i.e. $H^+ + e + O_{2ad} \rightarrow O + OH$, is assigned to be the major O_2 reduction channel on Pt; and the reaction is quenched at the high potentials due to the presence of the surface $O/OH/H_2O$ network that prevents the adsorption of bidentate O_2. We predict that a qualified ORR catalyst must allow bidentate O_2 adsorption under the equilibrium between adsorbed O and H_2O in solution at the concerned potential.

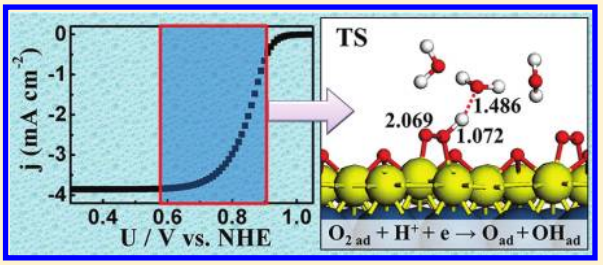

1. INTRODUCTION

Searching for efficient and economic cathode material for ORR in acid media ($O_2 + 4H^+ + 4e^- \rightarrow 2H_2O$, E_{eq} = 1.23 V vs SHE) must rank as one of the top concerns in fuel-cell applications.[1−3] Despite its high price and relative low catalytic activity for ORR, platinum is still an indispensable cathode material.[4] According to the observed Tafel curve, i.e., log(j) vs η (current vs overpotential) curve for ORR on Pt,[5−7] where two linear regions are identified, one below ~0.8 V (high η) with a Tafel slope of ~120 mV, another above ~0.8 V (low η) with a slope of ~60 mV,[8] it was realized that not only the intrinsic activity of the catalyst, e.g., at the low potentials (~120 mV Tafel slope), needs to be improved further, but also the rapid decrease of current above 0.8 V (~60 mV Tafel slope) must also be avoided. For the rational design of a new ORR catalyst, new experimental and theoretical techniques are urgently required to probe and understand the potential-dependent kinetics of this prototypical system. Notoriously, the major difficulty lies at the description of the special electrochemical environment from an atomic level, involving the solid−liquid interface, the electrochemical potential, and the coupled proton/electron transfer.

Although it is generally regarded that ORR is comprised of three key elementary steps, namely, O_2 bond breaking, O reduction, and OH reduction,[9] a great complexity arises owing to the unique electrochemical conditions and the exact nature of the rate-determining step in ORR is largely elusive.[10] For example, O_2 dissociation can proceed via either the direct bond breaking ($O_{2ad} \rightarrow O + O$),[11,12] or the proton-coupled bond breaking, $H^+ + e^- + O_{2ad} \rightarrow O + OH$.[13] Early experimental studies often assumed that O_2 dissociation is the rate-determining step as it was observed that the reaction order with respect to molecular oxygen is one.[13,14] Along this line, a dual-pathway mechanism for O_2 activation involving the direct and the proton-coupled bond breaking is often suggested in literature, both from experiment (e.g., Adzic's group[15]) and theory (e.g., the groups of Norskov,[16] Jacob,[10] Mavrikakis,[17] and Janik[18]). However, with the knowledge from recent surface science studies and theoretical calculations, this assumption is also questioned because O_2 bond breaking on bare Pt surfaces is found to be facile (can occur at low temperatures, e.g. 200 K).[19] Instead, other reaction steps were proposed as the rate-determining step, such as the reduction steps involving oxygen atom or hydroxyl groups[9,10] and the proton transfer to the compact layer.[20] Interestingly, in contrast to the large uncertainty on the overall mechanism, the kinetics of ORR, as represented by the measured Tafel curve, is relatively simple and definitive.

Specifically, for ORR at low potentials, the uncertainty lies mainly on whether the proton-coupled O_2 dissociation or the OH reduction is rate determining as both reactions involve only one electron transfer and thus can yield a Tafel slope of ~120

Received: April 11, 2012
Revised: May 18, 2012
Published: May 22, 2012

mV according to the Butler−Volmer relation ($j = j_0 e^{-\alpha\eta F/RT}$ and the Tafel slope $b = 2.3RT/\alpha F$, with α assumed to be 0.5 and b = 120 mV). On the other hand, ORR at the high potentials is more intriguing as a Tafel slope of ∼60 mV implies that more than one electron/elementary-step contribute to the overall kinetics. Damjanovic and co-workers[21] suggested that the switch of the Tafel slope is due to the variation of the activation barrier at different intermediate coverage that is linearly dependent on the potential, and the rate-determining step is unchanged, being the proton-coupled O_2 dissociation step. By fitting the experimental data with microkinetics equations, recently Wang et al.[22] suggested that the rate-determining step switches from the OH reduction (one-electron process) to the O reduction (two-electron process) with the increase of potential. A very high OH coverage (0.46 monolayer (ML) at the low potential) and O atom coverage (1 ML at the high potential) are however utilized to produce the best fit with the experimental rate, which are not consistent with recent theoretical calculations on Pt(111): the OH coverage and the O atom coverage are no more than 0.33 and 0.5 ML below 1.2 V, respectively. Because of these uncertainties on kinetics, some general questions in catalyst design remain open, such as why ORR activity is poor at the high potentials (i.e., above 0.8 V), and can Pt loading be reduced sufficiently toward a low cost catalyst?

In recent years, theoretical modeling based on density functional theory calculations has demonstrated its ability in providing detailed mechanism and kinetics for complex surface reactions. However, there are additional challenges in the theoretical modeling for electrochemical reactions such as ORR, compared to the reactions occurring in ultrahigh vacuum conditions. The first issue is the surface coverage at the reaction equilibrium. Under electrochemical conditions (for ORR it occurs at ∼0.8 V), the metal surface in contact with aqueous solution is often covered by a finite coverage of oxygen-containing species (O, OH, H_2O), especially at relative high potentials as encountered in ORR. Because the accurate measurement on the amount of these species remains challenging from experiment, the clean metal clusters/surfaces were often utilized as the model catalyst (e.g., the groups of Balbuena,[23−26] Jacob,[10,27,28] Goddard,[19,29] and Mavrikakis[17]), which however inevitably leads to an unrealistic estimation of the reaction kinetics for ORR. The second is the solvation. The presence of water environment on the electrode introduces a significant solvation energy contribution to the reaction kinetics. Especially, considering that the proton-coupled O_2 bond breaking involves the participation of a solvated proton and thus the proper treatment of the solvation is absolutely essential in order to compare the two likely bond breaking channels of O_2 on the same ground. Two classes of theoretical models were developed and utilized recently to include the solvation effect, namely the continuum solvation model (CM, without explicit water) and the explicit solvation by water layers (e.g., as implemented in the double-reference method[30]). Feng and Anderson noticed that the redox potentials of the reactions are very sensitive to the surface coverage by utilizing the CM method to evaluate the reversible redox potential of several O_2/H_2O related reactions, indicating that these two issues are strongly coupled in electrochemical systems. To date, because of these two major difficulties unique in electrochemical reactions, few theoretical studies were able to take into account all the important factors simultaneously in the same framework, not even mentioning the calculation of the theoretical Tafel curve for comparison with the kinetics from experiment. Obviously, to address fully the kinetics of ORR and thus reveal the mechanism from the atomic level, the computation of the Tafel curve from first principles is now the top concern.

To account for the contribution of electrochemical potential to the reactivity, it has been popular recently that a *neU* term (n is the number of the transferred electron) is applied as a correction to the reaction free energy for a electrochemical redox process.[31,32] However, this approach is based on thermodynamics and thus does not solve the puzzles in kinetics, for example, those on the Tafel curve. The thermodynamic approach does not contain the information of the transition state (TS), and the exact magnitude for n (the number of the transferred electron) at the TS is not known. In Marcus theory,[33] a 0.5 value for charge transfer coefficient is utilized to predict the TS position but it has never been calculated explicitly from first principles calculations for ORR.

Here by combining density functional theory (DFT) calculations with the recently developed periodic continuum solvation model based on modified-Poisson−Boltzmann (CM-MPB) electrostatics,[34,35] we determine the ORR Tafel kinetics and the polarization curve under electrochemical conditions from theory. We demonstrate that the proton-coupled O−O bond breaking is generally the rate-determining step in ORR at concerned potentials. The physical origin of the catalyst poisoning is identified as the competition of OH (from water oxidation) with O_2 in adsorption at high potentials. The theory here shows that it is possible to reduce markedly the utilization of Pt in active catalysts because only two Pt surface atoms are involved in the key O−O breaking step, while the rest of the surface Pt atoms are inactive, terminated by in situ produced O atoms.

2. CALCULATION METHODS

2.1. DFT Calculations. All DFT calculations were performed by using the SIESTA package[36] with numerical atomic orbital basis sets[37] and Troullier−Martins normconserving pesudopotentials.[38] The exchange-correlation functional utilized was at the generalized gradient approximation level, known as GGA-PBE.[39] The optimized double-ζ plus (DZP) polarization basis set with extra diffuse function was employed for metals. The orbital-confining cutoff was determined from an energy shift of 0.010 eV. The energy cutoff for the real space grid used to represent the density was set as 150 Ry. The Quasi-Newton Broyden method was employed for geometry relaxation until the maximal forces on each relaxed atom were less than 0.1 eV/Å and a criterion of 0.05 eV/Å has been utilized to fully converge the barrier of the concerned two competitive pathways. To correct the zero-point energy (ZPE), the vibrational frequency calculations were performed via the finite-difference approach. Transition states (TSs) of the catalytic reaction were searched by using the Constrained-Broyden-Minimization[40] and constrained-Broyden-dimer method.[41] The ORR at the solid/liquid interface has been modeled by using a periodic continuum solvation model based on the modified Poisson−Boltzmann equation (CM-MPB), which can take into account the long-range electrostatic interaction due to solvation. The periodic DFT/CM-MPB method has been utilized in our previous work on electro-/photocatalysis, and the detail of the implementation of the method is also described therein.[34,42,43] We utilize the solved H_3O^+ with its first solvation shell to model the reacting proton in solution, namely, $H_3O^+(H_2O)_3$ in bulk solution and $H_3O^+(H_2O)_2$ at the

dx.doi.org/10.1021/jp3034616 | J. Phys. Chem. C 2012, 116, 12696−12705

solid−liquid interface (the rest of the solution is represented by the CM-MPB model). At the solid−liquid interface, two of its H's of H_3O^+ are hydrogen bonded with the nearby water molecules and the remaining H interacts with the surface electronegative species such as O_2, O, and OH.

For the calculation of the surface adsorption structures and ORR reaction profile, we mainly utilized $(4 \times 2\sqrt{3})$ (16 Pt atoms per layer) six-layer slabs with adsorbates on both sides of the (111) surfaces. The middle two layers in the six-layer slab were held at the bulk truncated position and the other layers were fully relaxed. The TSs were searched on both sides of the slab. The Monkhorst Pack type of *k*-point sampling with a $(2 \times 2 \times 1)$ mesh was used in all calculations, and the denser $(4 \times 4 \times 1)$ *k*-point mesh was used to further check the convergence of reaction energetics. The accuracy of the calculated energetics was examined by benchmarking the results from SIESTA with those from the plane-wave methodology. For example, the O_2 free energy of adsorption ($G(O_2)$) (with reference to the free energy of the gas-phase O_2 at the standard state) at 1/16 ML on Pt(111) is calculated to be 0.74 eV from SIESTA, and it is 0.86 eV from the plane-wave method.

For Pt_3Ni skin alloy, we utilized the same $(4 \times 2\sqrt{3})$ six-layer slabs as pure Pt(111) with adsorbates on both sides of the surfaces. The composition of the layers utilized mimics those reported from experiment,[3] that is, the first layer is pure Pt; the second layer is Ni-rich with Pt:Ni = 1:1 and the layers underneath (bulk layers) with Pt:Ni = 3:1. Both the surface Pt layer and the Ni-rich layer were fully relaxed in optimization. All calculations for Pt_3Ni skin alloy were spin-polarized.

To derive the free energy reaction profile, we first obtain the reaction energy of each step (strictly speaking, Helmholtz free energy change (ΔF) at 0 K, 0 bar) that is directly available from DFT total energy (ΔE) after the ZPE correction. For elementary surface reactions without involving the adsorption/desorption of gaseous or liquid molecules, ΔF at 0 K, 0 bar is a good approximation to the Gibbs free energy (ΔG) as the temperature T and pressure p contributions at the solid phase are small. To compute the free energy change ΔG of elementary reactions involving gaseous or liquid molecules, such as oxygen, hydrogen, and water, the large entropy term at 298 K is essential to take into account. We utilize the standard thermodynamic data[44] to obtain the temperature and pressure contributions for the G of the aqueous H_2O and gaseous H_2, which are −0.57 eV (the entropy contribution is −0.22 eV in solution) and −0.31 eV compared to the total energy of the corresponding free molecule (E, 0 K), respectively.[45] The G of O_2 is derived as $G[O_2] = 4.92$ (eV) + $2G[H_2O] - 2G[H_2]$ by utilizing OER equilibrium at the standard conditions.

2.2. Theoretical Approach for Studying Electrochemical Systems. In our approach, the surface is explicitly polarized by adding/subtracting charges and the counter charge is distributed as point charge in 3D-grid according to the modified Poisson−Boltzmann equation.[34] The absolute electrochemical potential of the system can be calculated by computing the work function in solution and then referring it to the experimental work function of the standard hydrogen electrode (SHE, 4.4−4.8 from experiment and 4.6 V utilized in this work). This method has been utilized to calculate a variety of properties of metal surfaces, such as potential of zero charge and differential capacitance, and the calculated values show good agreement with experimental data (see the Supporting Information (SI), Table S1).

To study an electrochemical reaction under a constant potential as that encountered in experiment, we did a series of calculations with different surface charges for both the IS and the TS, e.g. generally from −1 |e| to 1 |e| with every 0.1 |e| increment. The reaction barrier can then be obtained for each fixed charge condition. Next, we need to link the computed surface charge with the electrochemical potential. For each state, the surface charge added can be linearly related to the computed electrochemical potential, as shown in Figure S1 in the SI. As introduced in our previous work, we assume that the electrochemical potential at the TS is the same as that at the IS considering that (i) the chemical reaction is a rare event and the occurrence of a single reaction on surface should not change the potential of the whole system and (ii) the unit cell utilized is already rather large with the reaction involving only 1/16−1/8 ML sites. With this assumption, we can directly utilize the calculated electrochemical potential at the IS as the potential for the reaction to occur. (In principle, it is always possible to enlarge the unit cell in slab calculations to let the computed potential at the TS and the IS be equal.) From our results, the potential difference between the IS and the TS is already rather small (i.e., 0.08 V) at the unit cell size of $(4 \times 2\sqrt{3})$ (16 Pt atoms per layer) for O−O dissociation (see Table S2 in the SI). This is largely due to the continuum solvation model, which can screen the lateral electrostatic interaction effectively.

For reactions involving H_3O^+ and electrons, such as the $O_2 + H^+ + e^-$ reaction, the potential of the system at the IS equals that of the same system without the H_3O^+ and electron (i.e., H_3O^+ and electron are infinitely far away) with the same approximation. In other words, the event that one H_3O^+ and electron approach a reactant at the reaction center does not change the potential of the whole system.

The DFT-calculated total energy must be corrected to compare the total energy of phases with different charges. Two extra energy contributions must be removed from the DFT total energy, namely, (i) the energy of the countercharge itself (E_{CQ}) and its electrostatic interaction with the charged slab ($E_{CQ\text{-}slab}$) and (ii) the energy of the excess charge in the slab (n_Q). For reactions involving the release of proton and electron, the reaction energy can be computed by referencing to the normal hydrogen electrode (SHE) in a manner proposed by the groups of Bockris[46] and Nørskov.[47] This is governed by $G_{proton+electron} = G(^1/_2H_2) - neU$, where e presents the transfer electron, n means the number of electrons, and U is the electrochemical potential vs SHE.

3. RESULTS

3.1. Surface Coverage at Reaction Equilibrium. At ORR steady state, the surface stays at a constant condition as dictated by the chemical potentials of reactant O_2 (gas phase), H_2O (solution), and acid (H^+, solute) under a certain electrochemical potential. To address the steady state kinetics, it is essential to know the in situ O coverage on the surface that can affect the kinetics of reactions significantly. Kinetically, this can be done by evaluating quantitatively the free energy barrier (ΔG_a) for the O-atom generation and the O-atom removal over various O-covered Pt(111) surfaces at a concerned potential. ΔG_a values of these two processes have to be comparable at the steady state. For the purpose of a fast screening, we first represent the O atom generation and removal processes by the O_2 direct dissociation ($O_2 \rightarrow 2O$) and the O atom reduction to OH ($O + H^+ + e^- \rightarrow OH$) reactions, respectively. In this way,

dx.doi.org/10.1021/jp3034616 | J. Phys. Chem. C 2012, 116, 12696−12705

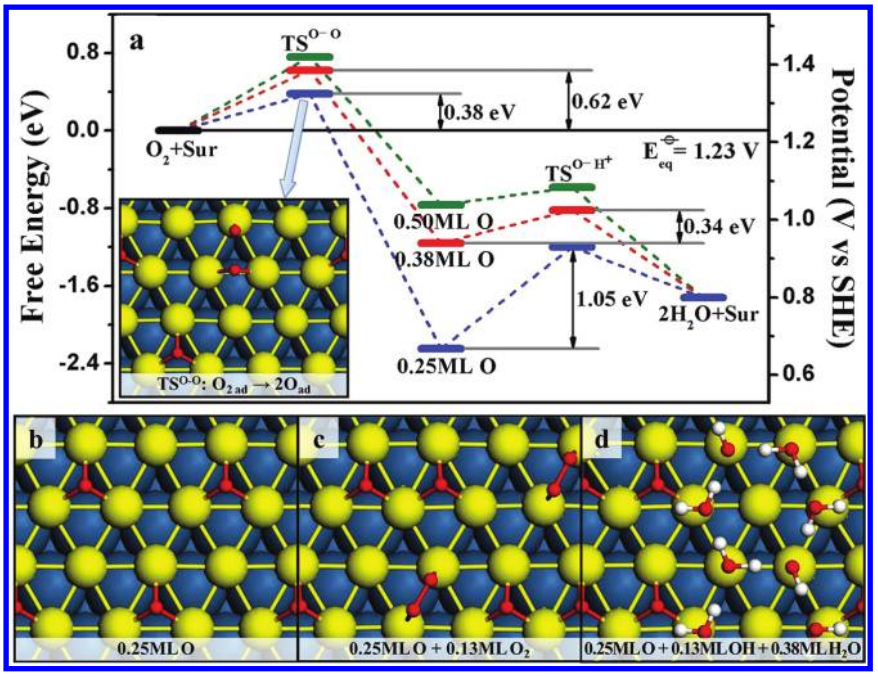

Figure 1. The steady-state kinetics analysis to determine the surface O coverage (a) and the key surface structures for ORR on Pt(111); (b) 0.25 ML O; (c) O_2/O phase: 0.25 ML O plus 0.125 ML O_2; (d) OH/H_2O/O phase: 0.25 ML O, 0.125 ML OH and 0.375 ML H_2O.

the potential effect on the overall reaction is taken into account by considering the free energy stability of the final product H_2O with respect to the reactant O_2 and the ΔG_a of the O removal (O_2 dissociation is assumed to be not potential dependent as no explicit electron transfer is involved). The O coverage estimated will then be validated by performing a complete reaction pathway search and kinetics analysis.

As shown in Figure 1a (the electrochemical potential is set at 0.8 V for illustration), O_2 dissociation into atomic O on Pt(111) at 0.125 ML O coverage is a highly exothermic process (by >1.2 eV in ΔG) and is kinetically facile (ΔG_a = 0.38 eV). (Because of the finite unit cell utilized, the dissociation of one O_2 per cell will increase the surface O coverage by 0.125 ML and the final surface O coverage is 0.25 ML). This is consistent with the general knowledge that O_2 dissociates facilely on bare Pt at low temperatures. On the other hand, the subsequent reduction of O atoms on the 0.25 ML O covered surface to restore the 0.125 ML O is kinetically more difficult with the overall ΔG_a being 1.05 eV at 0.8 V. This indicates that the surface O atom coverage will build up to 0.25 ML. In contrast, the O_2 dissociation becomes increasingly difficult for O coverages above 0.25 ML with the calculated ΔG_a being above 0.62 eV (0.62 eV is for O_2 dissociation at 0.25 ML), while ΔG_a for the O removal decreases significantly to 0.34 eV on a 0.38 ML O covered surface. Once the O coverage is at or above 0.38 ML, the removal of the additional surface O atoms will be kinetically much faster than the uptake of the surface O atoms. Obviously, because of the large gap in ΔG_a for reactions occurring below and above the 0.25 ML O covered surface, a steady state surface O coverage in between 0.25 and 0.38 ML is generally the most favorable for ORR on Pt(111) over a wide potential range, i.e., from 0.6 to 1.0 V from Figure 1 (the possibility for the concurrent water oxidation at high potentials is not considered here and will be addressed later). A 0.25 ML O coverage is therefore identified as the low limit for the surface O coverage and hereafter utilized as the initial surface O coverage for investigating the ORR kinetics.

The most stable configuration for 0.25 ML O on Pt(111) is a $p(2 \times 2)$ structure with each O occupying a fcc 3-fold hollow site without the surface Pt atom being shared (Figure 1b) and thus one per four Pt atoms is free of bonding with O, where the newly arrived O_2 prefers to adsorb and undergoes subsequent reduction. Both the decrease and the increase of O coverage will change the local concentration of the free Pt atoms and affect the activity of surface reactions markedly, as reflected in the calculated ΔG_a of O_2 dissociation and O reduction in Figure 1. We found that O_2 molecules can adsorb chemically on the 0.25 ML O covered Pt(111) with the adsorption energy being 0.44 eV: as shown in Figure 1c, at saturation there are 0.125 ML O_2 coadsorption with 0.25 ML O atoms, denoted as the O_2/O phase. In the phase, the O atoms, initially at a $p(2 \times 2)$ structure, adopt a more densely packed structure to accommodate the bidentate adsorbed O_2, which adsorb on two atop sites of Pt atoms.

At the high potentials, water oxidation on surface becomes inevitable (the reverse reaction of O atom reduction).[48] Quantitatively, it is essential to determine the OH emergence potential as controlled by the equilibrium potential of $H_2O \rightarrow OH^* + H^+ + e^-$. By examining the relative stability (free energy difference) of various possible OH adsorbed phases, we found that above 0.88 V an OH/H_2O mixed ring structure becomes more stable compared to the O_2/O phase, forming a 0.25 ML O + 0.125 ML OH + 0.375 ML H_2O structure, denoted as the OH/H_2O/O phase, as shown in Figure 1d. From our calculations, in order to accommodate the additional OH, the adsorbed O_2 must be removed from the O_2/O coadsorption structure because the adsorbed OH tends to form strong H-bondings with neighboring H_2O molecules and pin these H_2O molecules onto the surface. The overall equilibrium for the phase change can be summarized as O_2/O/Pt + $(H_2O)_2 \rightarrow$ OH/H_2O/O/Pt + $O_{2(g)}$ + H^+ + e^- with $E_{eq}^{(OH)}$ being 0.88 V. Apparently, owing to the competitive adsorption of OH with O_2 (no O_2 adsorption is possible on the OH/H_2O/O phase), an additional energy cost is required to remove OH species first

dx.doi.org/10.1021/jp3034616 | J. Phys. Chem. C 2012, 116, 12696−12705

to allow ORR at the high potentials. We will show that this will change markedly the Tafel behavior of ORR.

3.2. ORR Mechanism. On the O_2/O phase, we have investigated all the likely oxygen reduction channels leading to H_2O formation. Two different pathways were identified that are distinguishable according to how the O atom is generated, namely, (i) O−OH dissociation pathway via the proton-coupled O_2 bond breaking ($O_2 + H^+ + e^- \rightarrow O + OH$) and (ii) O−O dissociation pathway via the direct O_2 bond breaking ($O_2 \rightarrow 2O$). The participation of proton in ORR has been taken into account in our investigations for comparison with reaction kinetics measured in acidic media (e.g., pH ∼0 in experiment). In particular, the presence of a solvated proton nearby O_2 was found to facilitate the O_2 dissociation slightly (by ∼0.07 eV in ΔG_a). The obtained reaction free energy profile for the lowest energy pathway at the typical working potential, 0.8 V, and the key intermediates are illustrated in Figure 2 and the kinetic data

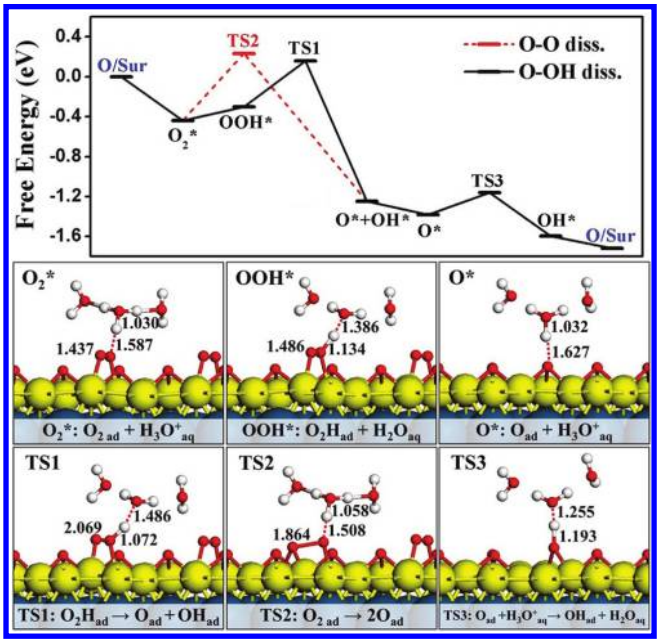

Figure 2. Free energy profile for ORR on Pt(111) at 0.8 V and the structural snapshots of O_2, OOH, adsorbed O, TS1 (O−OH dissociation), TS2 (O−O dissociation) and TS3 (O reduction).

for computing the free energies are summarized in Table 1 (the free energy profile and the kinetic data at the high potential limit, 0.96 V, are included in the SI, Figure S2 and Table S3).

In the O−OH dissociation pathway, the adsorbed O_2 is first reduced to a metastable OOH state. This is a facile equilibrium, $O_2 + H_3O^+ + e^- \leftrightarrow [OOH{-}OH_2]$, and the newly formed OOH is highly acidic, forming a very short contact (1.39 Å) with a nearby H_2O (see Figure 2, OOH*). Next, OOH can undergo the O−OH bond breaking and at the TS (**TS1** in Figure 2), the O atom and OH sit on two atop sites of Pt with the dissociating O−O distance being 1.98 Å at 0.8 V. After the dissociation, the O atom moves to a nearby 3-fold hollow site and the OH remains at the atop site. The calculated overall barrier is 0.60 eV at 0.8 V by comparing the free energy of the TS1 with respect to that of the adsorbed O_2 molecule.

On the 0.25 ML O precovered surface, the reduction of the newly formed O and OH (the local coverage is thus above 0.25 ML) are generally facile at 0.8 V. The lowest energy pathway for the reduction of O and OH is via the stepwise reduction by

Table 1. Calculated Free Energies of Elementary Steps in ORR on Pt (111) at 0.8 V

elementary steps	ΔE	$\Delta H(0\rightarrow 298\ K)$	ΔZPE	$-T\Delta S$	$-\|e\|U$	ΔG
O−O dissociation path (0.8 V)						
$sur + O_{2(g)} \rightarrow O_{2ad}$	−1.04	−0.09	0.05	0.64	0.00	−0.44
$O_{2ad} \rightarrow O{-}O_{TSad}$	0.74	0.00	−0.07	0.00	0.00	0.67
$O{-}O_{TSad} + H^+_{ad} + e^- \rightarrow O_{ad} + OH_{ad}$	−2.69	0.00	0.26	0.15	0.80	−1.48
$O_{ad} + OH_{ad} + H^+ + e^- \rightarrow O_{ad} + H_2O$	−0.77	0.10	0.26	−0.52	0.80	−0.14
$O_{ad} + H_2O + H^+ + e^- \rightarrow TS3 + H_2O$	−0.70	0.00	−0.03	0.15	0.80	0.22
$TS3 + H_2O \rightarrow OH_{ad} + H_2O$	−0.48	0.00	0.05	0.00	0.00	−0.44
$OH_{ad} + H_2O + H^+ + e- \rightarrow sur + 2H_2O$	−0.76	0.10	0.26	−0.52	0.80	−0.12
O−OH dissociation path (0.8 V)						
$sur + O_{2(g)} \rightarrow O_{2ad}$	−1.04	−0.09	0.05	0.64	0.00	−0.44
$O_{2ad} + H^+ + e^- \rightarrow OOH_{ad}$	−0.84	0.00	0.03	0.15	0.80	0.14
$OOH_{ad} \rightarrow O{-}OH_{TSad}$	0.51	0.00	−0.05	0.00	0.00	0.46
$O{-}OH_{TSad} \rightarrow O_{ad} + OH_{ad}$	−1.36	0.00	−0.05	0.00	0.00	−1.41
$O_{ad} + OH_{ad} + H^+ + e^- \rightarrow O_{ad} + H_2O$	−0.77	0.10	0.26	−0.52	0.80	−0.14
$O_{ad} + H_2O + H^+ + e^- \rightarrow TS3 + H_2O$	−0.70	0.00	−0.03	0.15	0.80	0.22
$TS3 + H_2O \rightarrow OH_{ad} + H_2O$	−0.48	0.00	0.05	0.00	0.00	−0.44
$OH_{ad} + H_2O + H^+ + e^- \rightarrow sur + 2H_2O$	−0.76	0.10	0.26	−0.52	0.80	−0.12

directing reacting with the solvated proton and electron in the Heyrovsky mechanism. The calculated ΔG_a of O atom reduction is only 0.22 eV (the structure of the TS, **TS3**, also shown in Figure 2) and that for the subsequent OH reduction is less than 0.1 eV. It might be mentioned that the indirect reduction of O/OH by an adsorbed H atom (i.e., Volmer−Tafel mechanism) has also been considered, i.e., $H^+ + e \rightarrow H$; $H + O/OH \rightarrow O/H_2O$, and it was found that the overall barrier of the two-step reduction is much higher compared to that of the direct Heyrovsky mechanism, apparently because H on the surface is much less stable compared to the solvated proton and electron at high potentials.

In competition with the O−OH dissociation pathway, the O−O dissociation pathway is energetically also likely. At the TS of the O_2 direct bond breaking (**TS2**, Figure 2), the O−O bond length of the adsorbed O_2 increases to 1.86 Å, with one O at the bridge site and another O sitting on the atop site where the presence of H_3O^+ nearby helps to stabilize the atop O. ΔG_a of the O−O dissociation is slightly higher (0.07 eV) than the O−OH dissociation pathway at 0.8 V. After the O−O bond breaking, an O and a OH are obtained with the atop O being spontaneously reduced to OH at 0.8 V. The subsequent reduction steps are the same as those in the OOH pathway mentioned above.

By comparing the direct and the proton-coupled O_2 bond breaking channel, we notice that the two channels have a similar free energy barrier at 0.8 V, the difference being only 0.07 eV from our DFT/CM-MPB calculations. While this is apparently consistent with the most suggested two-channel mechanism for O_2 activation, we will show in the next section that the two channels have distinct dependence on the

dx.doi.org/10.1021/jp3034616 | J. Phys. Chem. C 2012, 116, 12696−12705

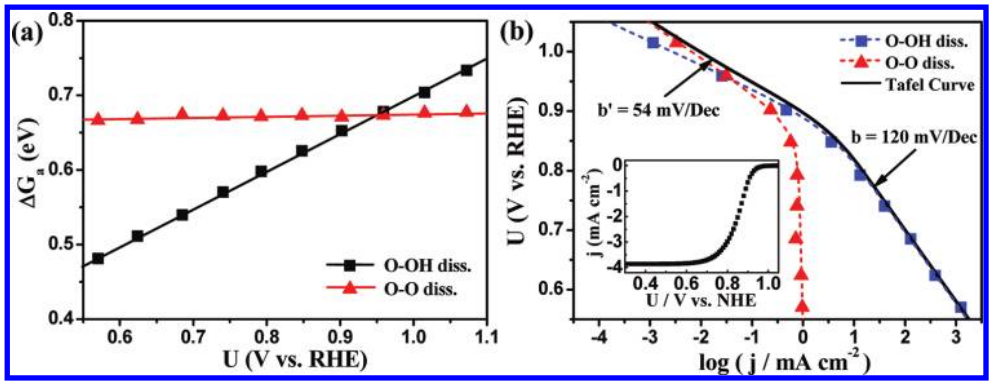

Figure 3. Plots for the computed free energy barrier vs potential (U) of two reaction channels (a), and the overall Tafel curves contributed from two reaction channels (b). The current−voltage (polarization current) curve is shown in the inset, with the maximum limiting current at the low potentials being ∼−3.9 mA/cm^2 as determined from experiment.[1]

electrochemical potential and because of this the proton-coupled O_2 bond breaking always dominates the O_2 activation pathway in the regime of concerned potentials (i.e., from 0.6 to 0.9 V).

It is also of interest to compare our calculated energetics with those reported in previous literatures. However, as also mentioned in the introduction, a large difference in the calculated barrier for the O_2 activation has been reported in the literature, essentially from almost zero to ∼0.7 eV,[9] not least because both the surface coverage and the solvation effect are critical to the exact value of ORR kinetics. Using small clusters, Anderson et al. first calculated the activation energies for O_2 and OOH dissociation on Pt_2 and found that OOH dissociation possesses a much lower energy barrier (0.06 eV) compared to O_2 dissociation,[49] while Ma and Balbuena reported a OOH dissociation energy barrier of 0.60 eV on a Pt_{12} cluster.[23] Jacob et al. studied OOH dissociation on a three-layer Pt_{35} cluster and reported a calculated energy barrier of 0.74 eV.[27] Using a clean Pt(111) slab, Hyman et al. reported an activation barrier for OOH dissociation of 0.22 eV,[50] similar to that (0.16 eV) reported by Mavrikakis and co-workers.[17] Without the solvation effect and coadsorbates, it was generally found that O_2 direct dissociation (e.g., barrier 0.6−0.7 eV[17,19] in the (2 × 2) cell) is less favorable than the OOH dissociation channel (e.g., below 0.3 eV). One step further, Rossmeisl and co-workers recently calculated OO and OOH dissociation in the presence of coadsrobed H_2O and OH (a first static water layer (i.e., short-ranged) is considered) and found the barrier varies from 0.37 to 0.73 eV.[51] Goddard and co-workers reported that the solvation effect included by a continuum solvation model (i.e., long-ranged) can reduce the O_2 dissociation barrier from 0.58 to 0.27 eV, and the OOH dissociation barrier from 0.17 to 0 eV on the clean Pt(111).[19] According to our studies, it should be emphasized that to treat properly the proton-coupled O_2 bond breaking channel, both the short-ranged nearby water molecules (the explicit solvation) and the long-range solvation (the implicit solvation) are essential. Apparently, this is largely due to the participation of the solvated proton in the reaction process. The so-called OOH entity in ORR is in fact a solvated [OO−H−OH_2] complex, reflecting the highly proton-like nature of H in OOH. In other words, it is not correct to represent the proton-coupled O_2 bond breaking simply by the dissociation of a standalone OOH without considering the O_2 protonation step and the solvation effect.

3.3. Kinetics and the Tafel Curve. From Figure 2, we can see that the TSs of the O−O or O−OH bond breaking dictate the highest energy position in the free energy profile and thus these O−O bond breaking steps should be the rate-determining steps in ORR, inconsistent with the general picture from Figure 1 for the O coverage above 0.25 ML. The subsequent elementary steps, the stepwise hydrogenation from O to H_2O, are facile (not rate-controlling) apparently due to the finite O coverage condition. The large lateral repulsion from coadsorbed O atoms above 0.25 ML coverage helps the reduction of additional Os to H_2O.

To further understand the Tafel kinetics of ORR, it is crucial to analyze how ΔG_a of these O−O bond breaking reactions varies against the potential. To this end, we have calculated the barrier of the reactions under different surface charges (charged slab) using the CM-MPB approach. The electrochemical potential of the reaction at a fixed surface charge can then be correlated with the computed ΔG_a by relating the electrochemical potential to the surface charge[34] (see calculation detail and SI, Figure S1). Figure 3a shows that the calculated ΔG_a of OOH dissociation decreases linearly with the increase of potential U, while ΔG_a of O_2 dissociation is rather constant over the potential range investigated. The ΔG_a of the two pathways is equal at ∼0.95 V. By fitting linearly the barrier−overpotential relation ($\Delta G_a = \Delta G_a^0 - \alpha F\eta$; $\eta = 1.23 - U$), we can deduce that the charge transfer coefficient α is 0.50 and 0.02 for O−OH and O−O dissociation, respectively. Importantly, the determined α, 0.5, for O−OH dissociation confirms the general assumption that α is 0.5 for the single electron transfer elementary reaction. For O−O dissociation, the reaction does not involve electron transfer explicitly and consistently, the calculated α is close to zero.

On the basis of the above DFT results, it is possible to further deduce the ORR Tafel kinetics by using microkinetics. As written in eq 1, the overall current j_k of ORR can be considered as a sum comprised of both reaction pathways (j_{OO} and j_{OOH}). For each reaction channel, the current j can be written as eqs 2−3, where A is the preexponential factor ($k_BT/h = 6.25 \times 10^{12}$ at 300 K from classic TS theory), ΔG_a is the DFT calculated free energy barrier of the rate-determining step, S is the total surface area, θ_{O_2} is the coverage of O_2, and $\theta_{O_2,max}$ is maximally 3/8 ML on the 0.25 ML O covered surface with respect to the available Pt sites. The realistic θ_{O_2} at the working potentials can be derived as eq 3, where the $\exp[F(U - E_{eq}^{(OH)})/RT]$ term takes into account the change of O_2 coverage with potential as modulated by the O_2/O/Pt +

dx.doi.org/10.1021/jp3034616 | J. Phys. Chem. C 2012, 116, 12696−12705

$(H_2O)_2 \rightarrow OH/H_2O/O/Pt + O_2(g) + H^+ + e^-$ equilibrium ($E_{eq}^{(OH)}$ = 0.88 V).

$$j_k = j_{OO} + j_{OOH} \quad (1)$$

$$j = FS^{-1}N_A^{-1} \times A \exp(-\Delta G_a/RT)\theta_{O_2}[H^+] \quad (2)$$

$$\theta_{O_2} = \theta_{O_2,max} \times p_{O_2} \times [H^+]/(p_{O_2} \times [H^+] + \exp(F(U - E_{eq}^{(OH)})/RT)) \quad (3)$$

Using eqs 1−3, we can plot the theoretical Tafel curves and the current−voltage curve for ORR at different electrochemical potentials as shown in Figure 3b (using p_{O_2} = 1 and $[H^+]$ = 0.1). The calculated current is in general consistent with those measured in experiment on Pt(111) surface in $HClO_4$ solution (where no specific adsorption of anions happens): at 0.8 V, log(j) is ∼1.1 from this work and ∼1.5 from experiment.[52] (Note that this (0.4 = 1.5−1.1) is a very small difference from the theoretical point of view considering that the 0.1 eV barrier difference will lead to the deviation of log(j) by 1.7.) Two linear regions can be distinguished with the slope switch occurring at ∼0.85 V and the Tafel slope is fitted to be 120 mV and 54 mV below and above ∼0.85 V, respectively.

From our data, we can easily identify that at the high overpotentials (below 0.85 V) the electric current j is dominantly contributed from the one-electron O_2 reduction step in the O−OH pathway, the proton-coupled O−O bond breaking (see Figure 3b). Because $\Delta G_{a(OOH)}$ is sensitive to the potential, the O−OH pathway becomes much more favorable than the O_2 dissociation at the high overpotentials.

On the other hand, at the low overpotentials from 0.85 to 1.0 V, the current j is a sum of both the O_2 and the OOH dissociation pathways as the two reactions are close in ΔG_a (within 0.1 eV). The value of the Tafel slope depends sensitively on the potential window utilized in the fitting, being from 45 to 60 mV. Importantly, the physical origin for the switch of the Tafel slope can now be clearly identified: it is the site blocking of the adsorbed OH due to water oxidation above 0.88 V that increases markedly the overall charge transfer coefficient of ORR and the Tafel slope.

3.4. Analyses and Discussion. Finally, it is of interest to analyze why the O−OH dissociation is highly potential dependent whereas O−O dissociation is not. Apparently, the two reactions share the same IS (adsorbed O_2 with solvated proton) and the difference must lie in the located TSs. For the IS, we have plotted the projected density of states (pDOS) (Figure 4a) onto the 1s(H) of the solvated proton and onto the 5d of a surface Pt atom at two different potentials, namely, 0.79 and 1.02 V. The energy levels are with respect to the same solution level (at the middle of the vacuum in slab calculations). It can be seen that with the increase of potential (i.e., the change of the Fermi level with respect to the reference level in solution), the energy levels of surface states will be stabilized accordingly, while that for the solvated proton remains constant, where the major bonding peak of H 1s at the ISs is invariant with respect to the change of potential, always being around −15 eV, as shown in Figure 4a,b. This is reasonable as the solvated proton locates away from the surface and the change of the Fermi level (potential) does not affect its energy level to a large extent.

At the TSs, as shown in Figure 2, the major structural difference between the two TSs (TS1 and TS2) occurs at the

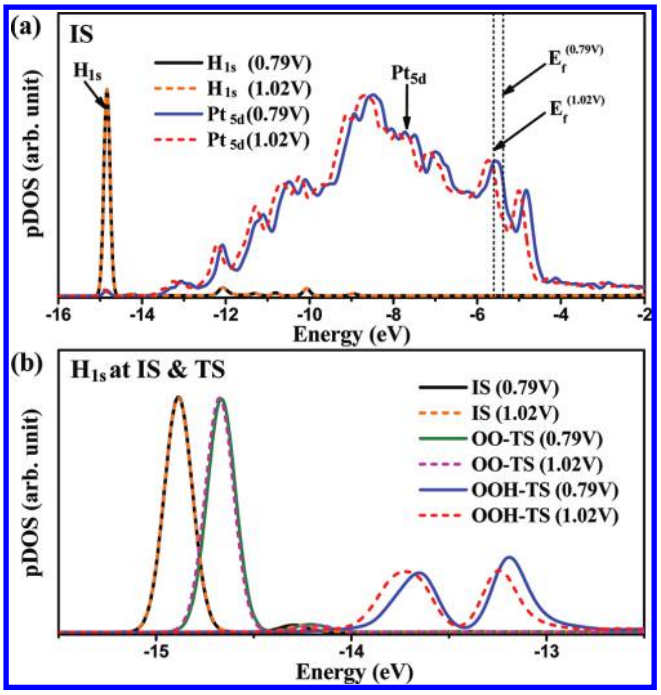

Figure 4. (a) Projected density of states (pDOSs) onto 1s of the H in H_3O^+ and 5d of the surface Pt at ISs. (b) pDOSs onto 1s of the reacting H in H_3O^+ for ORR following two different pathways. The energy zero is defined by the solution level and the Fermi level (E_f) at ISs are indicated, which vary with the change of potential. The major bonding peak of H_{1s} at the ISs (at ∼−15 eV) is invariant with the change of potential (because H_3O^+ at ISs is away from the surface), shown in both panels a and b.

position of the reacting H of H_3O^+. In TS1, the H attaches to O_2 (forming OOH), while in TS2, the H remains largely in the H_3O^+. It is therefore critical to examine how the localized states of the H respond to the variation of the potential. To this end, we further analyzed the pDOS on the 1s of H at the TSs at the two different potentials, focusing on the variation of the H_{1s} state with respect to the change of potential. We found that for O_2 dissociation, the major bonding peaks of H remain overlapping largely at two different potentials investigated, which is in line with the fact that the H is still the solvated proton above the surface. On the other hand, for the O−OH dissociation, the major peak of H_{1s} states splits into two peaks at the TS (as the H now links two Os) at −14 to −13 eV. Specifically, the peak position shifts down to the lower energy on going from 0.79 to 1.02 V, indicating that the reacting H interacts now strongly with the metal surface (with the increase of potential, the states of the catalyst surface will shift down in energy with respect to solution level as shown in Figure 4a Pt_{5d}). Fundamentally, the shift in H_{1s} states in the O−OH channel originates from the net electron transfer from the surface to the reacting H, while there is no net electron transfer (from surface to H_3O^+) in the O−O dissociation channel. It is the redox nature of the O−OH dissociation that leads to the sensitivity of its barrier to the electrochemical potential.

By reproducing the Tafel and polarization curve of ORR on Pt from first principles, we can now address some key issues in ORR kinetics. First, we identify a critical O coverage, 0.25 ML, for ORR on Pt by analyzing the reaction kinetics and at this coverage the O_2 molecule can adsorb and react. It would be interesting to predict what is the highest possible potential a catalyst can operate for ORR. On Pt(111), further adding the O

dx.doi.org/10.1021/jp3034616 | J. Phys. Chem. C 2012, 116, 12696−12705

atom on 0.25 ML coverage, one can determine the ΔG of the O/H_2O equilibrium, $H_2O + nO/sur \rightarrow (n+1)O/sur + 2H^+ + 2e^-$ (n counts as the number of O at 0.25 ML), is zero at 0.88 V from DFT, defined as the differential adsorption free energy of a newly arrived O atom ($\delta G_{O|0.88V} = 0$) with respect to H_2O in solution. All the calculated data for δG_O on Pt(111) are thus calculated and listed in Table 2 by only considering the O/H_2O

Table 2. Differential Adsorption Free Energies of O and O_2 Adsorption Free Energy on Pt(111) and Pt_3Ni Skin-Alloy at Different O Coverage Conditions (Considering only $H_2O + nO/Pt \rightarrow (n+1)O/Pt + 2H^+ + 2e$ Equilibrium)

O coverage	$\delta G_{O\|1.23V}$[a] /eV	$G_{ad}(O_2)$[b]/eV	U[c]/V
	Pt(111)		
0.06	−1.29	−0.69	0.59
0.13	−1.27	−0.73	0.60
0.19	−1.27	−0.70	0.60
0.25	−1.26	−0.44	0.60
0.31	−0.70	−0.43	0.88
0.38	−0.73	−0.24	0.86
0.44	−0.54	**−0.06**	**0.96**
0.50	−0.51	>0	0.98
	Pt_3Ni skin alloy		
0.06	−0.81	−0.35	0.83
0.13	−0.82	−0.59	0.82
0.19	−0.86	−0.49	0.80
0.25	−0.88	−0.14	0.79
0.31	−0.18	−0.21	1.14
0.38	−0.25	**0.02**	**1.10**
0.44	−0.01	>0	1.23

[a]The differential adsorption free energy of a newly arrived O atom on the O covered surface with respect to molecular O_2 (i.e., equivalent to H_2O in solution at 1.23 V and the standard state). [b]O_2 adsorption free energy on the O covered surface. [c]At the potential U, $\Delta G = 0$ ($\delta G_{O|U} = 0$) for $H_2O + nO/Pt \rightarrow (n+1)O/Pt + 2H^+ + 2e$, calculated by using $U = 1.23 + \delta G_{O|1.23V}/2$.

equilibrium. This equilibrium would dictate the lowest limit of O atom coverage under electrochemical conditions (as the O chemical potential in O_2 is higher than that in H_2O below 1.23 V, the presence of O_2 will certainly increase the O coverage). In previous work,[31,32] one generally uses this equilibrium to derive the surface phase diagram (metal surface in contact with H_2O). As we are interested in the highest possible O atom coverage when the O_2 can still adsorb, it is convenient to utilize this equilibrium as a simple tool to search for the lowest limit of the O coverage at the high potentials.

Table 2 shows that on Pt(111) the adsorbed O at 0.25 ML and H_2O in solution achieve equilibrium at ∼0.88 V, that is, the extra 0.06 ML O added onto 0.25 ML (in total 0.31 ML) is in equilibrium with H_2O at 0.88 V. Once increasing the potential, we can see the rapid accumulation of O coverage, e.g. the 0.44 ML O is in equilibrium with H_2O at 0.98 V, when the O_2 adsorption free energy is only marginally below zero, −0.06 eV. From our mechanism, because O_2 adsorption and the subsequent O−OH bond breaking involve two surface Pt atoms (a bidentate structure as seen in Figure 2) and compete with the adsorbed O atom for surface free Pt sites, *a qualified ORR catalyst must therefore allow bidentate O_2 adsorption when $\delta G_{O|U} = 0$ at the concerned potential U*. This fact can be simply extended to predict the starting potential (the low overpotential end) of a catalyst. On Pt, the bidentate O_2 adsorption is only likely below the O coverage 0.44 ML (see Table 2), where U = 0.96 V for achieving $\delta G_{O|U} = 0$, and indeed the starting potential for ORR on Pt is around 0.96 V.

Following this simple rule, we have calculated a Pt_3Ni skin alloy system (see calculation detail for the model), as inspired by recent experimental and theoretical studies.[3,53,54] We found that by alloying Ni with Pt, the O coverage on the surface is much reduced and the bidentate O_2 adsorption on the surface becomes infeasible until ∼1.10 V. This indicates that the starting potential of such a Pt_3Ni catalyst can reach 1.10 V (see Table 2), ∼0.15 V higher than pure Pt, inconsistent with the observed higher activity in experiment. It can be concluded that the key for achieving the high activity in ORR is to reduce the atomic O coverage while at the same time allowing O_2 bidentate adsorption.

Second, we demonstrate that reaction channel via proton-coupled O_2 bond breaking is the major mechanism for Pt catalyst, in which the active site involves essentially only two Pt atoms in the rate-determining step and thus a massive decrease of Pt utilization is theoretically likely. The intrinsic activity of the ORR catalyst is determined by the ability to break the O−O bond. On Pt, it is the precoverd O atoms that significantly increase the barrier of O−O bond breaking due to the large lateral repulsion between O_2 and O atoms (see Figure 1). Certainly, the reduction of O atom coverage is one possible means for improving the intrinsic activity of ORR catalyst, as already demonstrated in PtM skin alloys mentioned above.[35,55] Alternatively, a possible design of new ORR catalyst might be the introduction of electropositive ligands/cations in the catalyst to enhance the O−O bond breaking,[56,57] which could be promoted by the attraction due to the electropositive species.

4. CONCLUSIONS

This work utilizes the DFT-based periodic continuum solvation model in the framework of modified-Poisson−Boltzmann electrostatics to calculate the Tafel kinetics of ORR on Pt, aiming to settle down the reaction mechanism and resolve the key issues on the potential-dependent kinetics. For the first time the Tafel curve and the polarization curve of ORR can be calculated, and compared systematically with those observed in experiment. Both the slope and the switch in the curvature are reproduced from theory. Since the Tafel curve represents perhaps the most important kinetic information available from experiment, this theoretical work provides important insight into the proton-coupled electrochemical reaction at the atomic level and demonstrates that the computational electrocatalyst evaluation/screening is now reachable by kinetics. Specifically, the main conclusions of the work are outlined as follows.

(i) The O coverage at the reaction equilibrium, i.e. 0.25 ML, is identified from ORR kinetics on Pt at the concerned potentials, e.g. ∼0.8 V. The equilibrium O coverage, as dictated by both the O_2 activation and the electrochemical potential, is vital to the ORR mechanism as it affects significantly the O_2 adsorption and the subsequent activity. We show that a qualified ORR catalyst at the working potentials must allow bidentate O_2 adsorption.

(ii) The theoretical Tafel curve shows two linear regimes, one below ∼0.85 V with a slope of 120 mV and another above ∼0.85 V with a slope of 54 mV. The ORR activity is quenched above 0.96 V on Pt(111). These are consistent with the general findings in experiment.

dx.doi.org/10.1021/jp3034616 | J. Phys. Chem. C 2012, 116, 12696−12705

(iii) The proton-coupled O−O bond breaking, i.e. $H^+ + e^- + O_{2ad} \rightarrow O + OH$ channel, is the major mechanism for ORR on Pt catalyst, in which the active site involves essentially only two Pt atoms in the rate-determining step and thus a massive decrease of Pt utilization is theoretically likely. The redox nature of the proton-coupled O−O bond breaking leads to the strong potential dependence of the reaction and consequently a Tafel slope of 120 mV at the low potentials.

(iv) The switch of Tafel curvature above ∼0.85 V is due to the formation of hydroxyl groups on the surface, which competes with the adsorption of molecular O_2. The water itself thus acts as the poisoning species at the high potential, when each hydroxyl group on the surface will pin at least two nearby water molecules forming a stable first layer H-bonding network that together with adsorbed O atoms terminates fully the surface. How to avoid the production of hydroxyl at the high potentials is thus a key challenge toward reducing the high overpotential of ORR.

■ ASSOCIATED CONTENT

Supporting Information

Additional information on the CM-MPB method; the free energy diagram, and the data for ORR kinetics at 0.96 V. This material is available free of charge via the Internet at http://pubs.acs.org.

■ AUTHOR INFORMATION

Corresponding Author

*E-mail: zpliu@fudan.edu.cn.

Notes

The authors declare no competing financial interest.

■ ACKNOWLEDGMENTS

This work is supported by the National Nature Science Foundation of China (20825311, 21173051, 21103110), the 973 program (2011CB808500), the Science and Technology Commission of Shanghai Municipality (08DZ2270500), and the Program for Professor of Special Appointment (Eastern Scholar) at Shanghai Institute of Higher Learning.

■ REFERENCES

(1) Wu, G.; More, K. L.; Johnston, C. M.; Zelenay, P. *Science* **2011**, *332*, 443−447.

(2) Snyder, J.; Fujita, T.; Chen, M. W.; Erlebacher, J. *Nat. Mater.* **2010**, *9*, 904−907.

(3) Stamenkovic, V. R.; Fowler, B.; Mun, B. S.; Wang, G. F.; Ross, P. N.; Lucas, C. A.; Markovic, N. M. *Science* **2007**, *315*, 493−497.

(4) Gasteiger, H. A.; Markovic, N. M. *Science* **2009**, *324*, 48−49.

(5) Xiong, L.; Kannan, A. M.; Manthiram, A. *Electrochem. Commun.* **2002**, *4*, 898−903.

(6) Miyatake, K.; Omata, T.; Tryk, D. A.; Uchida, H.; Watanabe, M. *J. Phys. Chem. C* **2009**, *113*, 7772−7778.

(7) Murthi, V. S.; Urian, R. C.; Mukerjee, S. *J. Phys. Chem. B* **2004**, *108*, 11011−11023.

(8) Markovic, N. M.; Ross, P. N. *Surf. Sci. Rep.* **2002**, *45*, 121−229.

(9) Tian, F.; Anderson, A. B. *J. Phys. Chem. C* **2011**, *115*, 4076−4088.

(10) Keith, J. A.; Jacob, T. *Angew. Chem., Int. Ed.* **2010**, *49*, 9521−9525.

(11) Damjanov, A; Dey, A.; Bockris, J. O. M. *J. Electrochem. Soc.* **1966**, *113*, 739−746.

(12) Krasilshchikov, A. I. *Zh. Fiz. Khim.* **1963**, *37*, 531−537.

(13) Damjanov, A; Brusic, V. *Electrochim. Acta* **1967**, *12*, 615−&.

(14) Ross, P. N. *J. Electrochem. Soc.* **1979**, *126*, 78−82.

(15) Wang, J. X.; Uribe, F. A.; Springer, T. E.; Zhang, J. L.; Adzic, R. R. *Faraday Discuss.* **2008**, *140*, 347−362.

(16) Norskov, J. K.; Rossmeisl, J.; Logadottir, A.; Lindqvist, L.; Kitchin, J. R.; Bligaard, T.; Jonsson, H. *J. Phys. Chem. B* **2004**, *108*, 17886−17892.

(17) Ford, D. C.; Nilekar, A. U.; Xu, Y.; Mavrikakis, M. *Surf. Sci.* **2010**, *604*, 1565−1575.

(18) Yeh, K. Y.; Janik, M. J. *J. Comput. Chem.* **2011**, *32*, 3399−3408.

(19) Sha, Y.; Yu, T. H.; Liu, Y.; Merinov, B. V.; Goddard, W. A. *J. Phys. Chem. Lett.* **2010**, *1*, 856−861.

(20) Tripkovic, V.; Skulason, E.; Siahrostami, S.; Norskov, J. K.; Rossmeisl, J. *Electrochim. Acta* **2010**, *55*, 7975−7981.

(21) Sepa, D. B.; Vojnovic, M. V.; Vracar, L. M.; Damjanovic, A. *Electrochim. Acta* **1987**, *32*, 129−134.

(22) Wang, J. X.; Zhang, J. L.; Adzic, R. R. *J. Phys. Chem. A* **2007**, *111*, 12702−12710.

(23) Ma, Y.; Balbuena, P. B. *Chem. Phys. Lett.* **2007**, *447*, 289−294.

(24) Wang, Y. X.; Balbuena, P. B. *J. Phys. Chem. B* **2005**, *109*, 14896−14907.

(25) Wang, Y. X.; Balbuena, P. B. *J. Chem. Theory Comput.* **2005**, *1*, 935−943.

(26) Li, T.; Balbuena, P. B. *Chem. Phys. Lett.* **2003**, *367*, 439−447.

(27) Jacob, T. *Fuel Cells* **2006**, *6*, 159−181.

(28) Jacob, T.; Goddard, W. A. *ChemPhysChem* **2006**, *7*, 992−1005.

(29) Sha, Y.; Yu, T. H.; Merinov, B. V.; Shirvanian, P.; Goddard, W. A. *J. Phys. Chem. Lett.* **2011**, *2*, 572−576.

(30) Filhol, J. S.; Neurock, M. *Angew. Chem., Int. Edit.* **2006**, *45*, 402−406.

(31) Fang, Y. H.; Liu, Z. P. *J. Phys. Chem. C* **2009**, *113*, 9765−9772.

(32) Rossmeisl, J.; Norskov, J. K.; Taylor, C. D.; Janik, M. J.; Neurock, M. *J. Phys. Chem. B* **2006**, *110*, 21833−21839.

(33) Marcus, R. A. *J. Electroanal. Chem.* **1997**, *438*, 251−259.

(34) Fang, Y. H.; Liu, Z. P. *J. Am. Chem. Soc.* **2010**, *132*, 18214.

(35) Wei, G. F.; Liu, Z. P. *Energy Environ. Sci.* **2011**, *4*, 1268−1272.

(36) Soler, J. M.; Artacho, E.; Gale, J. D.; Garcia, A.; Junquera, J.; Ordejon, P.; Sanchez-Portal, D. *J. Phys.: Condens. Matter* **2002**, *14*, 2745−2779.

(37) Junquera, J.; Paz, O.; Sanchez-Portal, D.; Artacho, E. *Phys. Rev. B* **2001**, *64*, 9.

(38) Troullier, N.; Martins, J. L. *Phys. Rev. B* **1991**, *43*, 1993−2006.

(39) Perdew, J. P.; Burke, K.; Ernzerhof, M. *Phys. Rev. Lett.* **1996**, *77*, 3865−3868.

(40) Wang, H. F.; Liu, Z. P. *J. Am. Chem. Soc.* **2008**, *130*, 10996−11004.

(41) Shang, C.; Liu, Z. P. *J. Chem. Theory Comput.* **2010**, *6*, 1136−1144.

(42) Shang, C.; Liu, Z. P. *J. Am. Chem. Soc.* **2011**, *133*, 9938−9947.

(43) Li, Y. F.; Liu, Z. P.; Liu, L. L.; Gao, W. G. *J. Am. Chem. Soc.* **2010**, *132*, 13008−13015.

(44) *CRC Handbook of Chemistry and Physics*; 84th ed.; Lide, D. R., Ed.; CRC Press: Boca Raton, FL, 2003−2004.

(45) Liu, Z. P.; Jenkins, S. J.; King, D. A. *J. Am. Chem. Soc.* **2004**, *126*, 10746−10756.

(46) Bockris, J. O. M.; Khan, S. U. M. Surface Electrochemistry: A Molecular Level Approach; Plenum Press: New York, 1993.

(47) Rossmeisl, J.; Logadottir, A.; Norskov, J. K. *Chem. Phys.* **2005**, *319*, 178−184.

(48) Fang, Y. H.; Liu, Z. P. *J. Phys. Chem. C* **2010**, *114*, 4057−4062.

(49) Sidik, R. A.; Anderson, A. B. *J. Electroanal. Chem.* **2002**, *528*, 69−76.

(50) Hyman, M. P.; Medlin, J. W. *J. Phys. Chem. B* **2006**, *110*, 15338−15344.

(51) Rossmeisl, J.; Karlberg, G. S.; Jaramillo, T.; Norskov, J. K. *Faraday Discuss.* **2008**, *140*, 337−346.

(52) He, Q. G.; Yang, X. F.; Chen, W.; Mukerjee, S.; Koel, B.; Chen, S. W. *Phys. Chem. Chem. Phys.* **2010**, *12*, 12544−12555.

(53) Yang, Z. X.; Wang, J. L.; Yu, X. H. *Chem. Phys. Lett.* **2010**, *499*, 83−88.

(54) Matanovic, I.; Garzon, F. H.; Henson, N. J. *J. Phys. Chem. C* **2011**, *115*, 10640−10650.
(55) Greeley, J.; Stephens, I. E. L.; Bondarenko, A. S.; Johansson, T. P.; Hansen, H. A.; Jaramillo, T. F.; Rossmeisl, J.; Chorkendorff, I.; Norskov, J. K. *Nat. Chem.* **2009**, *1*, 552−556.
(56) Van, T. T. H.; Pan, C. J.; Rick, J.; Su, W. N.; Hwang, B. J. *J. Am. Chem. Soc.* **2011**, *133*, 11716−11724.
(57) Lefevre, M.; Proietti, E.; Jaouen, F.; Dodelet, J. P. *Science* **2009**, *324*, 71−74.